REVIEW

TRAIL: Simulating the impact of human locomotion on natural landscapes

Eduardo Alvarado[1] · Oscar Argudo[2] · Damien Rohmer[3] · Marie-Paule Cani[3] · Nuria Pelechano[2]

Abstract

Human and animal presence in natural landscapes is initially revealed by the immediate impact of their locomotion, from footprints to crushed grass. In this work, we present an approach to model the effects of virtual characters on natural terrains, focusing on the impact of human locomotion. We introduce a lightweight solution to compute accurate foot placement on uneven ground and infer dynamic foot pressure from kinematic animation data and the mass of the character. A ground and vegetation model enables us to effectively simulate the local impact of locomotion on soft soils and plants over time, resulting in the formation of visible paths. As our results show, we can parameterize various soil materials and vegetation types validated with real-world data. Our method can be used to significantly increase the realism of populated natural landscapes and the sense of presence in virtual applications and games.

Keywords Character animation · Natural phenomena

1 Introduction

Our physical actions inevitably change our environment, particularly when dealing with the effects of moving beings in highly diverse, natural scenes. For example, while a footprint on a beach will be washed away by the sea, taking frequently the same route over a grassy terrain will damage the plants, causing a reduction in their coverage and compacting the soil, resulting in the formation of a visible path (see Fig. 1). This is what naturalists call the "short-term or immediate impact" of human locomotion in contrast with longer-term effects over years that consider plant regrowth. The goal of this work is to simulate such an immediate impact.

Plausible physically based interaction between virtual characters and the environment can greatly enhance user experience and presence in games and immersive VR applications. In this regard, current video games typically model footprints using textures and the bending of blades of grass near characters using procedural approaches. However, permanent physical changes are ignored, trails are predefined and modeled in advance by artists, rather than emerging from the actual trajectories of characters. Therefore, our goal is to introduce the cause-and-effect relationship between character footsteps and trail formation, using a lightweight physical approach that allows us to achieve more plausible results while maintaining real-time performance. Furthermore, since our simulated results can be output as image data, they can also be integrated into texture-based pipelines to extend the visual results to larger scenarios.

In this paper, we present a holistic approach to simulate the interactions between human locomotion and its impact on soil and vegetation leading to the formation of trails in natural landscapes, thereby narrowing the gap between interactive animations and more realistic models of the environment in which our actions lead to visible effects. Our simulation uses a foot model, divided into heel and toe, to accurately compute the forces exerted when walking on both flat or sloping terrain (Sect. 3). It also includes a deformable plant model, with bending, degradation, and recovery to simulate the damage caused by the characters' footsteps (Sect. 4.1). Finally, a plastic terrain model is incorporated including a physically based simulation of soil compression, accumulation, and stabilization (Sect. 4.2). Our model also accounts for how vegetation mitigates the impact on the ground and increases soil cohe-

✉ Eduardo Alvarado
  ealvarad@mpi-inf.mpg.de

1 MPI Informatics, Saarland Informatics Campus, Saarbrücken, Germany

2 Universitat Politècnica de Catalunya, Barcelona, Spain

3 LIX, École Polytechnique/CNRS, Institut Polytechnique de Paris, Palaiseau, France

Fig. 1 Immediate changes in a land parcel due to the frequent passage of hikers

sion. Overall, our parameterized simulator can realistically replicate the impact of walking animations on different examples of soil and vegetation covers, and portray the dynamic alterations due to the cumulative impact of human locomotion that leads to the formation of trails (see Fig. 2). Our main contributions are:

- A lightweight physical system to improve foot positioning on soft terrains, enabling the adaptation of kinematic motion and computing accurate interaction forces.
- A dynamic plant model that can simulate its progressive damage due to stepping leading to coverage loss. The model is parameterizable and can mimic real plants.
- A foot-soil interaction model that accounts for the relative plant coverage and simulates loose ground stabilization and soil compaction.
- A customizable real-time simulator allowing the analysis and generation of local, image-based impact data under certain natural conditions.

While our method is general and could be extended to model the impact of wildlife, we focused on simulating the effects of humans or biped characters, which are most common in video games.

2 Related work

2.1 Character locomotion on natural grounds

While only handling flat and rigid grounds, early character animation methods either used physical models—requiring the design of motion controllers [18, 35], or lighter physical constraints with kinematic methods [6, 26, 38] to simulate character-scene interactions. More recently, data-driven methods addressed locomotion on uneven terrains [7, 19, 20, 30] but without tackling soft, dynamic grounds. In parallel, Deep RL gained popularity for its ability to learn motion controllers [24], but characters were never trained on deformable terrains.

Animating plausible locomotion in natural scenes also requires modeling the effects of the two-way interaction between the character and its surroundings. Still popular for real-time character animation [4, 34], Inverse kinemat-

ics (IK) was extended to characters evolving in complex environments thanks to specific foot placement strategies for both humanoids [21, 32] and multi-legged characters [1, 22]. Although a few human locomotion models used multiple joints for the feet [13, 25], they did not calculate the individual heel and toe rotations that would be required for computing interactions with uneven grounds. In addition to foot placement, two-way interactions might need some active adaptation of the character's gait, as was shown for locomotion under strong wind conditions [27] or across water bodies [5]. Closer to our concerns, two-way interactions with soft terrains were used to adapt real-time locomotion gaits [2], but the interaction forces derived from the motion model did not take into account the complex foot placement on slopes, leading to inaccurate exerted forces.
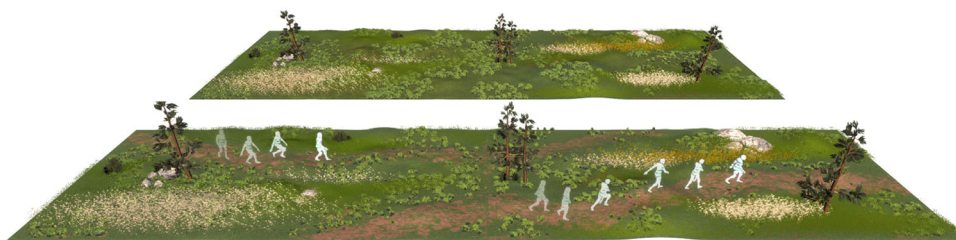
In this work, we combine kinematic animation data with a light physical model and procedural motion, enabling both, a more accurate foot placement and consequently, a precise exerted force computation on uneven grounds. Thanks to its genericity, our model can be applied to model varying ground deformations, and provide an efficient way to simulate data for the short-term human impact on natural landscapes.

2.2 Evolution of natural landscapes

Natural landscapes evolve over time under the effect of erosion [12, 15], vegetation growth [14] or climate [10, 33]. While abundant literature described landscape evolution under such factors and their combination [11], the range of graphical methods that have studied the impact of fauna or human population is limited. One of the most essential aspects when evaluating the impact of living beings on natural scenes is the short-term deformation caused on soft grounds, possibly covered with vegetation. Alvarado et al. [2] presented a terrain deformation approach to model human impact. However, height-field changes caused by the feet were not affected by the direction of the motion, the slope angle, or vegetation covering the ground. Concerning the latter, the effect that vegetation has on characters' gaits has been studied, for example, using procedural modifiers [32] or physics-based motion controllers [3]. However, none of these methods addressed the degradation effects that human locomotion caused on plants by damage to stems.

One of the major outcomes arising from the generation of these short-term changes is the formation of trails. However, modeling trail formation by encompassing plant damage and local erosion is challenging, as several scientific fields are involved, and data is lacking. Fortunately, a few real-world studies partly addressed the issue in the context of conserving natural environments: Cole et al. [8, 9] analyzed the response of several trampled vegetation types over time. We got inspiration from this study by modeling plant types based on their resistance and tolerance, i.e., their ability to

Fig. 2 Our simulation results are used to estimate the immediate impact of character locomotion on natural landscapes (top), including damage to vegetation and soft ground deformation. This leads to the progressive formation of trails (bottom)

Fig. 3 We adapt the orientation of each joint according to the distance to the ground (left), paying particular attention to situations where the tip of the foot makes contact before the heel (right)

recover after being degraded. More recently, Marion et al. [29] identified the main key factors for trail degradation and profiling, dominated by grade (ground angle) and dryness, which we account for in our model in terms of slope and ground material. Although the analysis of trail formation created over long periods of time is beyond the scope of this work, our approach aims to measure the short-term interactions occurring between humans and natural environments that are primarily responsible for creating longer-term effects.

3 Forces exerted by a walker on natural terrains

The first ingredient to model human impact on natural environments is to be able to compute, from any input locomotion and the mass of the walker, the force that the feet exert over time onto the vegetation and ground below. To launch such computation on realistic, motion-captured data—typically captured on flat, rigid grounds—the input kinematic motion needs to be adapted to the terrain. In this section, we introduce a new, two-joint foot model, which allows (i) to adapt the placement and orientation of the feet on the fly to match any targeted terrain and (ii) to compute the forces exerted on the contact surface over time.

In what follows, the input is a character model described as an animated kinematic skeleton to which a skinned mesh is attached. We also input the mass of the character and the position of its center of mass relative to the kinematic skeleton.

3.1 Slope-aware foot positioning

Unlike flat terrain where the contact surface between the ground and the feet is always the same at a given stage of the gait cycle, humans continuously adapt the placement of their feet on uneven terrains, e.g., by leaning on their toes to climb. This change of contact area according to the slope has a significant impact on the alteration of terrains, as shown by the distinct footprint shapes. We therefore introduce a model enabling precise heel and toe contact with uneven grounds.

We consider a foot model made of two joints: *heel* and *toe*, as illustrated in Fig. 3-left. Each joint is associated with
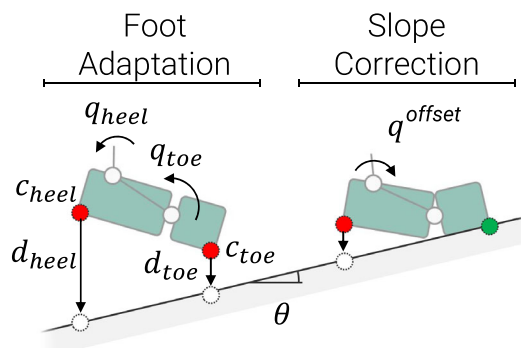
a position p_{heel} (resp. p_{toe}) and orientation represented as a quaternion q_{heel} (resp. q_{toe}). The foot is rigged with a 3D mesh, using a simple primitive or a more realistic model (e.g., a shoe). We further associate the two geometric extremities of the respective mesh, c_{heel} and c_{toe}, indicating the mesh points considered for detecting contact with the ground. We first apply the local alignment of each foot part as a continuous function of the vertical distance to the ground. Denoting q_{joint} for either heel or toe orientation, we consider:

$$q_{joint} = \text{SLERP}(q_{joint}^{kin}, q_{joint}^{\perp}, w_d),$$
$$w_d = \text{clamp}\left(1 - d_{joint}/d_{max}, 0, 1\right),$$
(1)

where q_{joint}^{kin} is the input orientation generated from the kinematic animation, $q_{joint}^{\perp}$ is the joint orientation orthogonal to the ground surface and preserving the local forward direction of the foot, d_{joint} is the distance between c_{joint} and its vertical projection on the floor, and d_{max} is a user-defined threshold describing the spatial extension of the influence of this smooth IK constraint.

On flat terrain, the character's heel is normally the first body part to touch the ground. However, this behavior might change on steep terrains, where the forefoot is the first contact point, leading to variations in the foot-ground plantar and dorsiflexion angles [37]. In this case, the character's toe is often used to support maintaining balance and moving forward and upward, while the heel remains above the ground at all times. We refine our two-joint model to represent this additional plantar and dorsiflexion in the ankle with q^{offset},

such as the foot pushes off with the toes when it gets closer to the ground, followed by raising the toes to clear the steep slope as it moves away. Let θ be the angle of the local slope of the terrain with respect to the horizontal direction, and θ_0 the minimum angle for which the foot can use only its toe as support. We apply the rotation q^{offset} of angle $\theta - \theta_0$ to q_{heel}:

$$q_{\text{heel}} \leftarrow q^{\text{offset}} \, q_{\text{heel}}. \tag{2}$$

This mechanism, illustrated in Fig. 3-right, leads to a smaller contact area onto the ground, thus generating increased local pressure, as explained in the next section.

3.2 Exerted forces during feet-to-ground contact

Inspiring by Alvarado et al. [2] force model in the case of a rigid foot, we estimate the force $\vec{F}_{\text{foot}}$ exerted by our new dual-joint foot on the ground as follows. We compute an impulse-based response from the input animation and convert it into a smooth time-varying force spread over a characteristic time interval τ:

$$
\begin{aligned}
\vec{F}_{\text{foot}} &= \alpha(\vec{F}_{\text{weight}} + \vec{F}_{\text{momentum}}), \\
&= \alpha \, (m \, \vec{g} + \vec{J}/\tau),
\end{aligned}
\tag{3}
$$

where α represents the percentage of weight and impulse spread between the left and right foot position, depending on the position of the character's center of mass [16], m is the character's mass and $\vec{g}$ is the gravity constant. $\vec{F}_{\text{momentum}}$ represents the required exerted force during the interval τ to establish a certain impulse: $\vec{J} = m \, \vec{v} \, (t_0 - \Delta t)$, where t_0 is the time of contact between the foot and the ground, Δt is the frame time interval, and $\vec{v} \, (t_0 - \Delta t)$ is the velocity of the foot evaluated at the frame immediately before impact. $\vec{F}_{\text{momentum}}$ is active only during the interval $[t_0, t_0 + \tau]$.

This force is exerted either by the heel, the toe, or both, depending on the contact surface over time. We consider that c_{heel} or c_{toe} are in contact with the ground when the distances to the ground $\|d_{\text{heel}}\|$, respectively $\|d_{\text{toe}}\|$ (see Fig. 3) fall below a user-defined threshold value ϵ, typically in the range of $[0.5, 1]$ cm. We evaluate the velocity $\vec{v}$ at the frame preceding the impact of the foot on the ground as:

$$
\vec{v} =
\begin{cases}
\vec{v}_{\text{heel}} & \text{if } d_{\text{heel}} < \epsilon \\
\vec{v}_{\text{toe}} & \text{if } d_{\text{toe}} < \epsilon \\
\vec{v}_{\text{centroid}} & \text{if } d_{\text{heel}} < \epsilon \text{ and } d_{\text{toe}} < \epsilon
\end{cases}
\tag{4}
$$

where $\vec{v}_{\text{centroid}}$ is the velocity at the center of mass of the foot.

As illustrated in Fig. 4, the procedural foot placement defined by Eqs. (1) and (2) influences the magnitude and direction of $\vec{v}$, and therefore $\vec{F}_{\text{momentum}}$, based on the adaptive motion of the foot and the resulting point of contact with
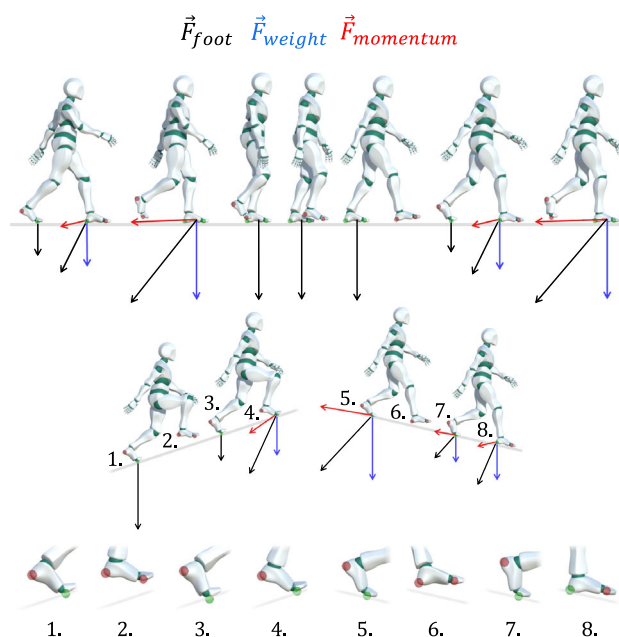
$\vec{F}_{foot}$ $\vec{F}_{weight}$ $\vec{F}_{momentum}$

Fig. 4 Interaction forces are exerted on the terrain for flat ground (top) and slopes (middle) at different gait stages. During the stance phase, the force exerted into the ground equals the weight supported by that foot ($\vec{F}_{\text{foot}} = \vec{F}_{\text{weight}}$). Modeling heel and toe contact events (bottom) helps evaluate accurate forces on uneven grounds

the ground. This is most noticeable on uneven terrain. For example, when walking uphill, characters use their toes to exert larger forces and push their bodies upward.

4 Impact on plants and soft grounds

As humans traverse a path, vegetation tends to degrade, leaving the bare ground exposed. This leads to more intense damage and progressive ground compaction for a repeated application of stress at the same location. In this section, we describe how we convert the character's exerted force into localized vegetation and natural ground responses.

4.1 Modeling vegetation

Damage to vegetation plays a crucial role when deforming the ground underneath. However, plants are resilient barriers: even when crushed underfoot, they can repair themselves and grow back over time. In addition, while protecting the soil by reducing direct contact, they also increase its cohesion thanks to their roots. We propose a dynamic plant model that depicts not only their deformation but also their change in robustness—referred to as *degradation* and *recovery*—, which models the damage generated in the plant over the short term.
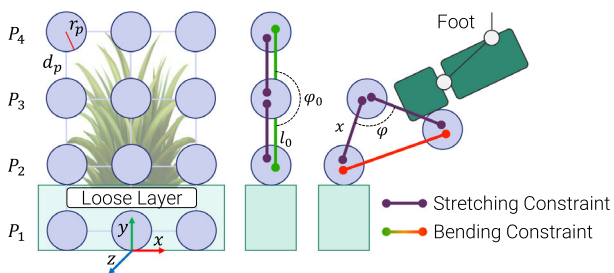
Fig. 5 A surface 2D plant-row model. Particles are vertically interconnected using stretching and bending constraints, enabling the model to retrieve its shape after trampling

4.1.1 Deformable plant model

As simulating the bending and breaking of individual plant stems would be costly, our model relies on an approximation using efficient Position-Based Dynamics (PBD) [31] to animate them. Our approach allows us to model vegetation instances in a variety of shapes, whether using 2D vertical surfaces or combining them to form a volumetric representation of the plant. Either way, our approach allows entire sets of plants to be simulated at once on the terrain surface, able to bend. These instances are created and placed on the ground with random orientations according to the nature and local density of plants.

A plant instance is characterized by its height h_p, width w_p and depth d_p. The shape is sampled using physical particles forming a 2D-or-3D grid structure and equipped with spherical rigid colliders of radius r_p (as illustrated in Fig. 5-left for the 2D case). To enable plants to retrieve their shape after any light interaction with the feet, we inter-connect particles using stretching C_s and bending C_b constraints, defined as:

$$C_s : l - l_0 = 0$$
$$C_b : \varphi - \varphi_0 = 0, \tag{5}$$

where l is the constrained edge length between horizontal, vertical, or diagonal particles, and φ is the constrained angle between consecutive edges in the horizontal, respectively vertical direction, l_0 and φ_0 being their initial values. In our model, increasing the horizontal l_0 decreases the density of particles since the vertical edges can be interpreted as distinct stems (see Fig. 5-middle-right). Stiffness parameters ε_s and ε_b for stretching and bending, respectively, are associated with each constraint. They are set to lower values along the horizontal edges (connecting neighboring stems) with respect to vertical ones, especially as the density of stems in the rows decreases. This induces the desired anisotropic behavior under deformation. For the 2D case, the first two lines of particles, located respectively at the root of the first

row, are not animated but serve to maintain the base in a stable, vertical position.

4.1.2 Dynamic degradation and recovery

When the character's foot comes close to the plant, collisions with the physical particles in the 2D-or-3D grid cause local changes of l and φ. We consider three cases based on the bending value φ concerning the degradation and rupture thresholds, ($\varphi_{\text{deg}}, \varphi_{\text{max}}$), respectively.

For a small bending ($\varphi < \varphi_{\text{deg}}$), the affected stem adopts a purely elastic behavior and returns to its original state when the foot moves away. In contrast, for a large bending ($\varphi > \varphi_{\text{max}}$), the stem is set to break and the associated constraint is disabled. Lastly, for intermediate deformations $\varphi \in [\varphi_{\text{deg}}, \varphi_{\text{max}}]$, the stem undergoes a temporal degradation or recovery process modeled by a time-varying angular stiffness ε_b:

$$\varepsilon_b \leftarrow \varepsilon_b - \mu_{\text{deg}} \, \Delta t \quad \text{while } \varphi \in [\varphi_{\text{deg}}, \varphi_{\text{max}}]$$
$$\varepsilon_b \leftarrow \varepsilon_b + \mu_{\text{rec}} \, \Delta t \quad \text{once } \varphi < \varphi_{\text{deg}} \tag{6}$$

where μ_{deg} and μ_{rec} are the plant-type related temporal degradation and recovery factors, and Δt is the time-step. If ε_b reaches 0 during this process, the stem is considered to be broken and the associated constraint is removed, as in the high-bending case. Inversely, if ε_b increases and reaches the maximum stiffness for this category of plants, the stem recovery process stops.

As a result, our stem degradation and recovery processes modify the plant elastic behavior; reducing ε_b makes the stem more flexible, thus more prone to bend beyond φ_{max} and break. As introduced in the next section, our plant model assimilates the ratio of remaining stems (active constraints) to the plant's health.

4.1.3 Increased ground cohesion due to vegetation

In addition to directly interacting with the walkers' feet, dense and healthy vegetation also strengthens the ground due to its root system. We model this using a "vegetation-induced stiffness" term E_v, which is added to the ground's Young modulus before computing the compaction under the feet. E_v is computed as follows.

We first compute a local strength ratio α_{veg} of vegetation, defined as the density of healthy, non-broken stems around a given point p, where the stems are assimilated to the vertical constraints of our deformable plant-row model:

$$\alpha_{\text{veg}}(p) = \frac{1}{N_{\text{veg}}} \sum_k^{N_{\text{veg}}} \left(1 - \frac{\| p - p_k \|}{w_p} \right) \alpha_{\text{veg}}^k, \tag{7}$$

where N_{veg} is the total number of plants whose center p_k is located in a circle of radius w_p around p, and $\alpha_{\text{veg}}^k = N_c/N_c^0$ is the strength ratio of a given plant k, with N_c the number of active vertical constraints, and N_c^0 its initial number at full plant health. A value of $\alpha_{\text{veg}}(p)$ close to 1 indicates locally dense and healthy, and therefore strong vegetation at point p, while a value close to 0 indicates sparse and/or broken vegetation.

Considering that healthy vegetation coverage would imply a maximum increase E_v^0, we define the increase of Young Modulus due to degraded vegetation as:

$$E_v(p) = \alpha_{\text{veg}}(p)\, E_v^0. \tag{8}$$

This value is used when computing the ground's response to foot pressure, as described next.

4.2 Plastic model for natural terrains

Consider a natural terrain whose upper soil layer of thickness L_0 is malleable enough to be affected by the pressure of the walker's foot while the ground remains rigid below. We present a new plastic model for the top layer, calculating both underfoot compression and lateral displacement of part of the loose soil. Our model takes into account not only the presence of the plant roots but also the movement of the feet and the direction of the slope, which allows us to model the cascading motion of the displaced material.

4.2.1 Ground compression

We use the linear stress–strain relation from [2] to compute the local ground compression at a point p of the foot contact area. But in contrast with this work, we increase the ground modulus E by the previously computed vegetation-induced term from Eq. (8):

$$E(p) = E_g(p) + E_v(p), \tag{9}$$

where $E_g(p)$ is the Young modulus at p, which may be obtained from geological data [17, 23].

The terrain being represented as a height field stored in a 2D grid, the soil's compression and carving ΔL at each grid cell experiencing foot contact is then derived from Hooke's law:

$$\Delta L = \sigma\, \frac{L_0}{E} = \frac{\vec{F}_{\text{foot}} \cdot \vec{n}_y}{A_{\text{contact}}}\, \frac{L_0}{E}, \tag{10}$$

where σ is the pressure stress, computed based on $\vec{F}_{\text{foot}} \cdot \vec{n}_y$, the component of the force $\vec{F}_{\text{foot}}$ orthogonal to the ground, and where the contact area A_{contact} is efficiently computed using ray-casting from a small sub-grid of the terrain's map,
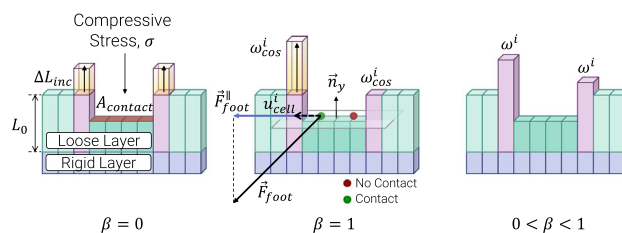

Fig. 6 Vertical cross sections of different accumulation models on an initially flat terrain. From left to right: uniform distribution, cosine distribution along a projection to the terrain's tangent plane of the direction of the force $\vec{F}_{\text{foot}}$ exerted by the foot, and our adaptive interpolation where the amount of anisotropy depends on the norm of the projection

centered on the foot: $A_{\text{contact}} = n_{\text{hits}}\, \text{cell}_{\text{length}}^2$, where n_{hits} is the number of cells where the foot intersects the ground.

Since loose soils are partly compressible, part of the material under the foot should move and accumulate nearby in the form of a small bump. [2] addressed this by evenly redistributing the amount of incompressible material under the foot (characterized by the ground's Poisson's ratio ν_g), to the 1-neighboring cells around the contact zone of total area A_{border}, leading to uniform bumps around the compressed region (see Fig. 6-left).

In the next section, we introduce an improved model, accounting for the orientation of the foot's pressure force with respect to the local terrain slope.

4.2.2 Anisotropic soil accumulation

Walking on steep terrain or pushing the feet hard on the ground throws soil material unevenly, leading to its nonuniform accumulation around the contact region. We introduce an anisotropic soil accumulation model that takes into account the local orientation of the foot force relative to the terrain. Let's call $\vec{F}_{\text{foot}}^{\parallel} = \vec{F}_{\text{foot}} - (\vec{F}_{\text{foot}} \cdot \vec{n}_y)\,\vec{n}_y$ the tangential component, with respect to the terrain, of the force exerted by the foot.

Being $\vec{F}_{\text{foot}}^{\parallel}$ the main direction of material projection, a purely anisotropic distribution of accumulated material could be modeled by using a positive cosine distribution law $\omega_{\cos}^i$ around it, as:

$$\omega_{\cos}^i = \max(\vec{F}_{\text{foot}}^{\parallel} \cdot u_{\text{cell}}^i, 0)\, /\, \|\vec{F}_{\text{foot}}^{\parallel}\|, \tag{11}$$

where u_{cell}^i is the unit vector between the force application position and the current cell i of the footprint border in A_{border}. This distribution is maximal and equals to one in cells aligned with $\vec{F}_{\text{foot}}^{\parallel}$, and smoothly decreases as the cosine of the angle between u_{cell}^i and $\vec{F}_{\text{foot}}^{\parallel}$. It vanishes when the cell is orthogonal or opposite to $\vec{F}_{\text{foot}}^{\parallel}$ (see Fig. 6-center). The anisotropic distribution ω^i is set to interpolate between a

distribution uniformly equal to 1, and this cosine distribution:

$$\omega^i = \beta \, \omega_{\cos}^i + (1 - \beta). \tag{12}$$

The anisotropic material accumulation in i-th cell is thus $\Delta L_{\rm inc}^i = \frac{\omega^i}{\sum_k \omega^k} \, \Delta L_{\rm inc} \, A_{\rm border}$. The value of the interpolation weight β is automatically computed from $\|\vec{F}_{\rm foot}^{\parallel}\|$. When $\|\vec{F}_{\rm foot}^{\parallel}\|$ is close to zero, the foot is applying an orthogonal force to the ground, so the distribution is set to isotropic ($\beta = 0$). Conversely, if $\|\vec{F}_{\rm foot}^{\parallel}\|$ is large (steep terrain or high speed for the character's foot), its tangential component pushes the material in the direction of this force. We then use the cosine distribution ($\beta = 1$). In the general case:

$$\beta = \min\left(\frac{\vec{F}_{\rm foot}^{\parallel}}{F_{\rm threshold}}, \, 1\right), \tag{13}$$

where $F_{\rm threshold}$ is a user-defined parameter giving the limit force magnitude above which a purely anisotropic distribution applies.

4.2.3 Terrain stabilization

Displaying stacks of material around the foot-ground contact area would be unrealistic. We use a height-field stabilization mechanism inspired by a sand-dune model [33] to calculate, at each time-step, a quasi-static equilibrium configuration. This method generates a physically valid configuration of the accumulated loose soil, depending on the local slope.

In a stable slope, the angle $\gamma^{(i,j)}$ between each pair of cells (i, j):

$$\gamma^{(i,j)} = \tan^{-1}\left(\frac{h_i^c - h_j^{c+1}}{\rm cell_{length}}\right) \tag{14}$$

is smaller than the so-called resting angle γ_r, a parameter that depends on the soil material. Thus, for a given frame, we look at each cell and its neighbors to check the local stability of the stack of material. If $\gamma^{(i,j)} > \gamma_r$, we transfer material from the cell i to its neighbors. Given the amount of material h to be distributed, each direct, lower neighbor j in the 1-ring receives a fraction $w_s^{(i,j)}$ of h proportional to the height difference:

$$w_s^{(i,j)} = \frac{(h_i^c - h_j^{c+1})}{\sum_j (h_i^c - h_j^{c+1})}. \tag{15}$$

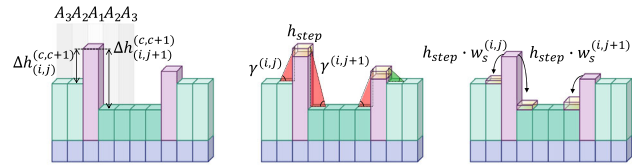Therefore, for each pair of cells (i, j), we use:

Fig. 7 Stabilization step, repeated until convergence. Height differences between neighboring cells are computed to estimate stabilization weights $w_s^{(i,j)}$ (left). Local slopes are classified between non-stable (in red) and stable (in green) (middle). Small amounts of material are moved (right)

$$\begin{cases} h_i^c \leftarrow h_i^c - h_{\rm step} \\ h_j^{c+1} \leftarrow h_j^{c+1} + w_s^{(i,j)} \, h_{\rm step} \end{cases} \text{if } \gamma^{(i,j)} \geq \gamma_r, \tag{16}$$

This stabilization process is executed starting from the border of the contact region A_1 and then in outward rings of increasing radius (increasing c values), until a stabilized state where $\gamma <= \gamma_r$ is reached (see Fig. 7). To avoid upward material transport, $w_s^{(i,j)}$ is clamped to positive values. Note that limiting material transfer between cells to a small constant height $h_{\rm step}$ limits temporal jittering of cell elevations. Otherwise, the material could be sent back and forth between two neighboring cells over several iterations before convergence to the slope resting angle. In our implementation, less than 10 stabilization steps are needed for $h_{\rm step} = 0.01$.

4.3 Impact data generation

We combined every presented component (from pressure forces on steep terrain to vegetation and ground responses), into a standalone simulator (Sect. 5.1), used to generate impact data. For each simulation, we store two maps to describe the landscape's initial conditions: the initial vegetation distribution expressed as the vegetation strength ratio $\alpha_{\rm veg}^{\rm in}$ in each cell, and a Young Modulus map $E_{\rm total}^{\rm in}$ accounting for both the nature of the ground and vegetation coverage (see Eq. (9)). During the simulation, we record at every new second the accumulated pressure stress generated by humans presence over a given time-interval $T_{\rm sim}$:

$$\sigma_{\rm acc}^{\rm out}(T_{\rm sim}) = \int_{T_{\rm sim}} \sigma(t) \, dt, \tag{17}$$

where $\sigma(t)$ is the instantaneous pressure stress from Eq. (10). Additionally, we store the simulated results corresponding to the terrain's compression and accumulation ($h_c^{\rm out}(T_{\rm sim})$, $h_a^{\rm out}(T_{\rm sim})$) relative to the original terrain height (thus modeling the deformation to be applied to the height map), and the final strength ratio of vegetation $\alpha_{\rm veg}^{\rm out}(T_{\rm sim})$ (see Fig. 8).
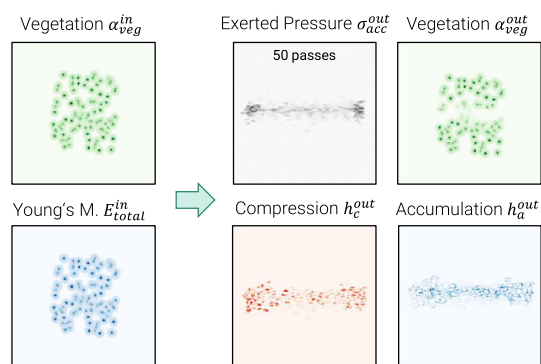
Fig. 8 Four simulated maps corresponding to the simulation of 50 consecutive human passes walking back and forth between left and right

5 Results and discussion

5.1 Standalone simulator

We developed our model as an independent simulator designed for use in gaming environments, particularly within serious games aimed at raising awareness about soil degradation for educational and environmental purposes. The character, which can be interactively controlled with a gamepad or keyboard, is animated using Motion Matching [7]. We also provide the possibility to define waypoints on the map serving as successive position targets, and the character's path between two waypoints can be procedurally generated with random variations. Simulation outcomes are instantly displayed and ground/vegetation parameters can be directly set, giving experts the capability to adjust them to the real values when known. Please refer to the supplemental video for more details on the simulator.

We implemented this simulator in *Unity* with C#. Our system has been tested using two terrain resolutions for the deformable height map, 512×512 and 256×256. The former runs at 30 FPS while the latter resolution achieves 60 FPS during the terrain deformation process only. Using this last height map resolution, we achieve a performance of 20 FPS (50 ms/frame) when we add 200 plant in the simulation, on a single-GPU workstation (*Intel Xeon*, ten cores at 3.70 GHz, *GeForce* RTX 3090). The main computational costs during the simulation are spent on the position-based deformation for multiple vegetation rows (55%), followed by the continuous contact area calculation along with terrain deformation (35%), and the animation system with procedural adaptation (10%). Note that these timings could be optimized by skipping the simulation of the plant instances far from the character.

To get a greater variety of landscapes, we have experimented with three different types of soil conditions, each corresponding to a different material behavior. In addition, two types of short vegetation were studied. The parameters

for ground and vegetation used throughout this work are reported in Table 1.

The simulated impact can be used to enrich natural environments and depict a more accurate evolution under the presence of characters for interactive applications. For Fig. 9, we run different simulations under diverse ground and vegetation conditions. A shader applies the simulated output to an artistically detailed, identical topography in real-time, using impact maps for ground deformation and billboards for vegetation density. Accelerated animations of these changes are shown in the supplementary video. This could be as well extended to larger terrain (see Fig. 2).

5.2 Validation of the soft ground model

In Fig. 10, we show the results of our terrain deformation model on flat ground. The characters use parametric SMPL models [28] to depict variable body shapes associated with different masses, which influence the resulting deformation. The average walking speed of each character is 1.3 m/s. For the character with $m = 75$ kg, the average pressure exerted by the feet at this relaxed walking pace is 20 kN, consistent with the experimental results reported in [36]. Using the same ground parametrization, we compare our new soil accumulation with [2] for left to right locomotion (see Fig. 11). Note the anisotropy of our foot track, consistent with both motion direction and soil stability laws.

Figure 12 shows the combined influence of motion direction and steep terrain slopes on footprints and provides a qualitative validation compared to real, sandy terrain: Walking up-hill (left) leads to smaller footprints (toe-only contact), with bumps opposite to the direction of motion; walking down-hill (middle) generates longer footprints due to sliding foot in contact with the ground, with sand bumps in the direction of motion; Finally walking sideways (right) results in foot-size footprints with bumps on the lowest side.

5.3 Validation of the vegetation model

Our simulator can be used to enhance interactive locomotion in natural landscapes for films and games, thanks to the use of PBD for modeling different types of plants and their dynamic behavior just after trampling (see Fig. 13 for a comparison between real and simulated deformations).

We also use our plant model to estimate the damage to vegetation due to trampling. We employ the real data reported in [8] to fine-tune and then validate our vegetation model. This study measured the effects of trampling on various types of vegetation, after different numbers of successive passages (25, 75, 200, and 500) on controlled land patches, reporting the relative plant coverage after two weeks—which they refer to as immediate effects of trampling—and after one year.

Table 1 Ground and vegetation parameters

Ground	Soft soil	Dry soil	Wet soil
E_g [MPa]	[0.7, 2]	[0.2, 0.5]	[0.3, 0.7]
ν_g	[0.1, 0.3]	[0.3, 0.4]	[0.2, 0.4]
γ_r [°]	[10, 15]	[5, 10]	[10, 15]
Vegetation	*Carex pensylvanica*	*Lycopodium lucidulum*	
E_v^0 [MPa]	7	10	
$(\varepsilon_b, \varepsilon_s)$ [s^{-1}]	(0.1, 1)	(0.08, 1)	
$(\varphi_{\deg}, \varphi_{\max})$ [°]	(10, 70)	(5, 50)	
(μ_{deg}, μ_{rec}) [s^{-1}]	(0.1, 0.1)	(0.1, 0.1)	

Fig. 9 Soft Soil with *Carex pensylvanica* (top row), Dry Soil (middle row) and Wet Soil (bottom row), both with *Lycopodium lucidulum*, after 1 (left), 75 (middle) and 200 passes (right). A custom shader enables lightweight rendering by modifying ground appearance and billboard density based on the simulated maps over time
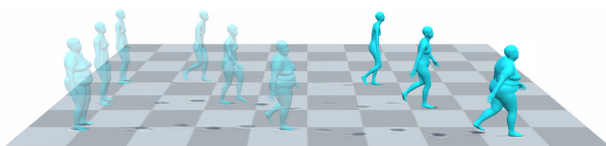
Fig. 10 Deformation of Dry Soil in flat terrain, whose settings are reported in Table 1. Compression, anisotropic accumulation and material stabilization are used to show the impact of SMPL characters [28] with $m = 50, 75$, and 100 kg
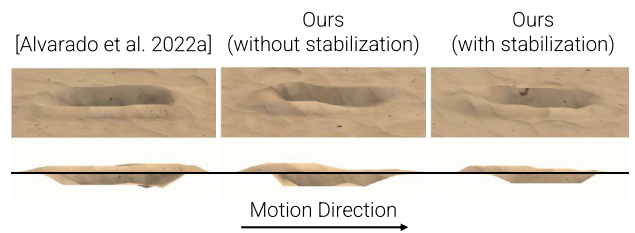
Fig. 11 Footprint profile comparison

To validate the short-term degradation and recovery of our plant model, we replicated the same experimental conditions, focusing on two of the originally reported plant types (*Carex pensylvanica* and *Lycopodium lucidulum*). For this experi-mental setup, we generate two simulations, each one with a vegetation-covered path containing 200 plant instances, each defined by a 2D shape of size 0.1×0.05 m^2, with particle radius $r_p = 0.005$ m and distance between particles
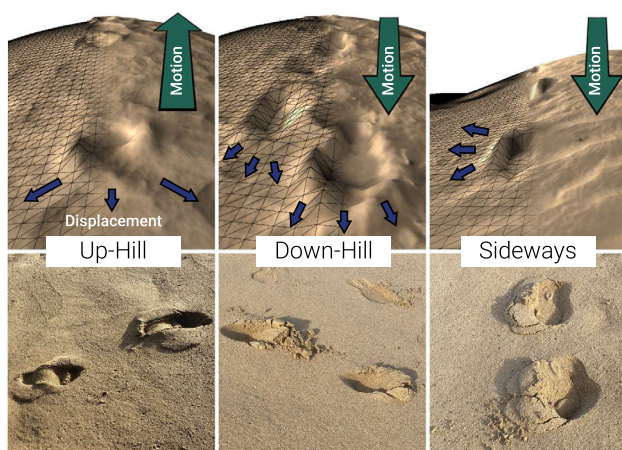
Fig. 12 Simulated foot tracks (top) vs. real ones (bottom) on a steep, sandy dune, respectively, for climbing up, going down, and a sidewalk. Green (resp. black) arrows show the direction of motion (resp the direction of projected sand)
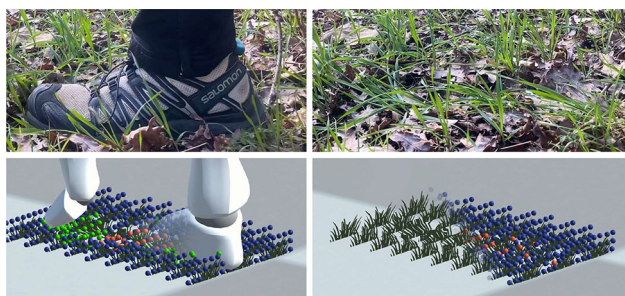

Fig. 13 Comparison between real (top), and simulated (bottom) dynamic plant deformation after trampling. The plant's bending behavior (shown here on aligned grass rows to make the direction of deformation more salient) makes them more resilient, and thus more apt to recover

Fig. 14 Short-term damage on *Carex pensylvanica* (top) and *Lycopodium lucidulum* (bottom)

Fig. 15 Comparison between our simulated vegetation cover and real data about immediate damage due to trampling [8]

Fig. 16 Walking on bare ground carves deeper footprints than with vegetation (top). Rendering without the plants (bottom)

$d_p = 0.015$ m. We use the regressive analysis in [8] provided on the immediate degradation effects to set the internal stiffness and threshold parameters as well as the degradation and recovery rates of our simulated plant model, which are reported in Table 1. Results illustrating the change in α_{veg} (introduced in Eq. (7)) after a certain number of passes are shown in Fig. 14.

A comparison of the real vegetation cover in [8] and our simulated conditions is shown in Fig. 15, demonstrating how our plant model captures well the immediate impact, even for moderate trampling. Note that this approach for parameter setting could be easily generalized given the corresponding data for a variety of plants. Finally, in Fig. 16, we show how damage to *Carex pensylvanica* affects, in our model, the terrain underneath it, due to the decreasing generalized Young Modulus.
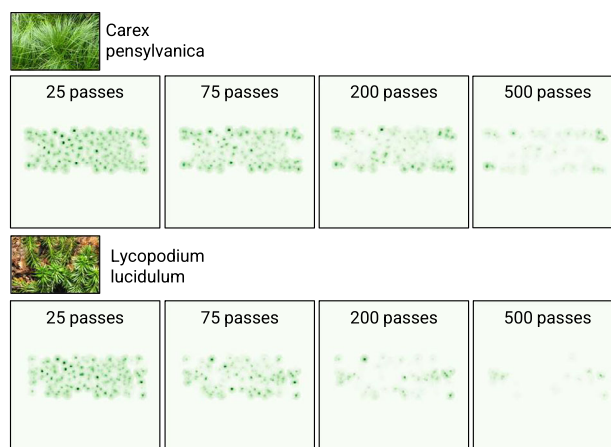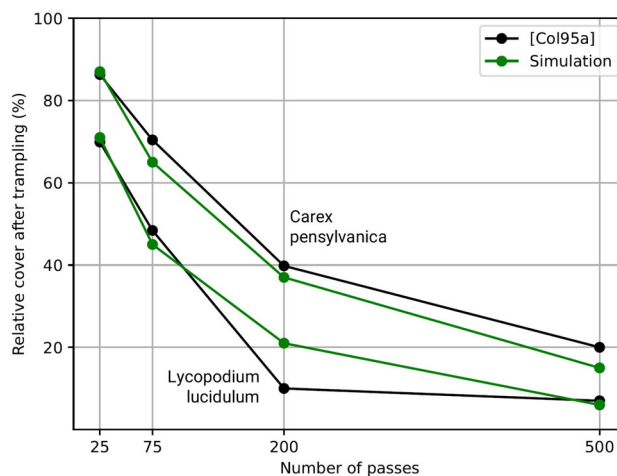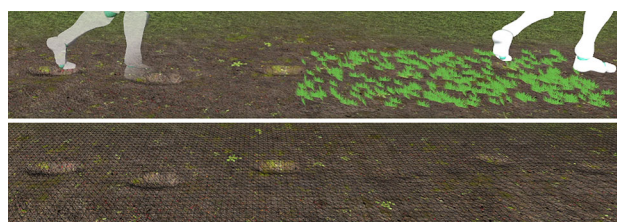
5.4 Discussion and limitations

The above results illustrated the advantages of our method relying on efficient interactive models and allowing plausible modeling of the temporal impact of human locomotion in natural environments. However, some approximations were made for performance:

Firstly, although efficient, our vegetation model could be improved by automatically optimizing its internal parameters based on real-world data for different plant species. The use of PBD for more complex, asymmetric deformable volumes tuned from the underlying plant strength and density should be explored. In addition, while our time-linear degradation and recovery models are easy to control, they would benefit from a more complex stress model, accounting for the quality of the surrounding soil (function of compaction) and the impact of climatic conditions. Another important aspect would be the long-term regeneration and regrowth of vegetation, which our approach does not consider and would allow us to have a more consistent model for trail evolution.

Second, our anisotropic soil accumulation approach considers the tangential force with respect to the terrain when the foot establishes contact. However, dragging material due to friction forces while the foot remains grounded is not considered. Its implementation would add further plausibility to the impact, enabling the simulation of more general categories of gaits, such as walk shuffling. In addition, modeling the accumulation of solid debris like gravel, or erosion and transport of bare ground due to rainfalls and other climatic conditions (such as temperature changes fracturing compacted ground) would also be needed for accurately predicting the long-term evolution of trails once vegetation has been damaged.

Finally, character behavioral modes encompass manual control or procedural routes. While it is beyond the scope of this paper, it would be very interesting to further explore the idea of autonomous characters whose decision-making is influenced by the evolution of the terrain, often making them take more accessible routes due to the lack of vegetation, and thus accentuating the degradation effect over time.

6 Conclusions and future work

In this work, we introduced a method to simulate short-term changes in populated, natural landscapes due to the presence of two-legged characters. We adapt input kinematic motion to establish accurate force interactions with the irregular ground, which in combination with deformable terrain and vegetation models, allows us to measure the local impact data on the surroundings. We integrate these individual tasks into a comprehensive simulator, enabling users to seamlessly input motion and environmental conditions, thereby facilitating the analysis of the resulting impact.

This work represents a first step toward a more accurate analysis of human influence on natural landscapes. Our methodology could be potentially extended with data-driven strategies, aiming to forecast the long-term evolution of wildlife scenes. Lastly, the method can be already integrated into standard texture-based pipelines in games and films, thereby highlighting the existence of virtual populations and creating more lively and diverse natural environments over time.

Author Contributions E.A. and O.A. carried out the main technical implementation. E.A. and O.A. wrote the main manuscript text and prepared figures, with continuous assistance from D.R., M-P.C., and N.P. E.A. prepared the supplementary material. All authors reviewed the manuscript.

Data Availability No datasets were generated or analyzed during the current study.

Declarations

Conflict of interest The authors declare no competing interests.

References

1. Abdul Karim, A., Gaudin, T., Meyer, A., Buendia, A., Bouakaz, S.: Procedural locomotion of multi-legged characters in dynamic environments. Comput. Animat. Virtual Worlds **24**(1), 3–15 (2012). https://doi.org/10.1002/cav.1467

2. Alvarado, E., Paliard, C., Rohmer, D., Cani, M.P.: Real-time locomotion on soft grounds with dynamic footprints. Front. Virtual Real. **3**, 3 (2022). https://doi.org/10.3389/FRVIR.2022.801856

3. Alvarado, E., Rohmer, D., Cani, M.P.: Generating upper-body motion for real-time characters making their way through dynamic environments. Comput. Graph. Forum **41**(8), 169–181 (2022). https://doi.org/10.1111/cgf.14633

4. Aristidou, A., Lasenby, J., Chrysanthou, Y., Shamir, A.: Inverse kinematics techniques in computer graphics: a survey. Comput. Graph. Forum **37**(6), 35–58 (2018). https://doi.org/10.1111/cgf.13310

5. Bermudez, L., Tessendorf, J., Zimmermann, D., Zordan, V.: Real-time locomotion with character-fluid interactions. In: Proceedings

of the 11th ACM SIGGRAPH Conference on Motion, Interaction and Games, MIG'18. Association for Computing Machinery, New York (2018). https://doi.org/10.1145/3274247.3274515

6. Boulic, R., Mas, R., Thalmann, D.: A robust approach for the control of the center of mass with inverse kinetics. Comput. Graph. **20**(5), 693–701 (1996). https://doi.org/10.1016/S0097-8493(96)00043-X

7. Clavet, S.: Motion matching and the road to next-gen animation. In: Game Developer Conference (GDC) (2016)

8. Cole, D.N.: Experimental trampling of vegetation. I. Relationship between trampling intensity and vegetation response. J. Appl. Ecol. **32**(1), 203–214 (1995)

9. Cole, D.N.: Experimental trampling of vegetation. II. Predictors of resistance and resilience. J. Appl. Ecol. **32**(1), 215–224 (1995)

10. Cordonnier, G., Ecormier, P., Galin, E., Gain, J., Benes, B., Cani, M.P.: Interactive generation of time-evolving, snow-covered landscapes with avalanches. Comput. Graph. Forum **37**(2), 497–509 (2018). https://doi.org/10.1111/cgf.13379

11. Cordonnier, G., Galin, E., Gain, J., Benes, B., Guérin, E., Peytavie, A., Cani, M.P.: Authoring landscapes by combining ecosystem and terrain erosion simulation. ACM Trans. Graph. **36**(4) (2017). https://doi.org/10.1145/3072959.3073667

12. Cordonnier, G., Jouvet, G., Peytavie, A., Braun, J., Cani, M.P., Benes, B., Galin, E., Guérin, E., Gain, J.: Forming Terrains by Glacial Erosion. ACM Trans. Graph. **42**(4) (2023). https://doi.org/10.1145/3592422

13. da Silva, D.B., Nunes, R.F., Vidal, C.A., Cavalcante-Neto, J.B., Kry, P.G., Zordan, V.B.: Tunable robustness: an artificial contact strategy with virtual actuator control for balance. Comput. Graph. Forum **36**(8), 499–510 (2017). https://doi.org/10.1111/cgf.13096

14. Gain, J., Long, H., Cordonnier, G., Cani, M.: Ecobrush: interactive control of visually consistent large-scale ecosystems. Comput. Graph. Forum **36**(2), 63–73 (2017). https://doi.org/10.1111/cgf.13107

15. Galin, E., Guérin, E., Peytavie, A., Cordonnier, G., Cani, M.P., Benes, B., Gain, J.: A review of digital terrain modeling. Comput. Graph. Forum **38**(2), 553–577 (2019)

16. Garcia, A.L.: Principles of animation physics. In: ACM SIGGRAPH 2012 Courses, SIGGRAPH'12 (2012)

17. Gerling, B., Löwe, H., Van Herwijnen, A.: Measuring the elastic modulus of snow. Geophys. Res. Lett. **44**, 11088–11096 (2017). https://doi.org/10.1002/2017GL075110

18. Hodgins, J.K., Wooten, W.L., Brogan, D.C., O'Brien, J.F.: Animating human athletics. In: Proceedings of the 22nd Annual Conference on Computer Graphics and Interactive Techniques, SIGGRAPH'95, pp. 71–78. Association for Computing Machinery, New York (1995). https://doi.org/10.1145/218380.218414

19. Holden, D., Kanoun, O., Perepichka, M., Popa, T.: Learned motion matching. ACM Trans. Graph. **39**(4) (2020). https://doi.org/10.1145/3386569.3392440

20. Holden, D., Komura, T., Saito, J.: Phase-functioned neural networks for character control. ACM Trans. Graph. **36**(4) (2017). https://doi.org/10.1145/3072959.3073663

21. Johansen, R.S.: Automated semi-procedural animation for character locomotion. Master's thesis, Aarhus Universitet, Institut for Informations Medievidenskab (2009)

22. Karim, A.A., Meyer, A., Gaudin, T., Buendia, A., Bouakaz, S.: Generic spine model with simple physics for life-like quadrupeds and reptiles. In: Bender, J., Kuijper, A., Fellner, D.W., Guerin, E. (eds.) Workshop on Virtual Reality Interaction and Physical Simulation. The Eurographics Association (2012). https://doi.org/10.2312/PE/vriphys/vriphys12/097-106

23. Klár, G., Gast, T., Pradhana, A., Fu, C., Schroeder, C., Jiang, C., Teran, J.: Drucker–Prager elastoplasticity for sand animation. ACM Trans. Graph. (TOG) **35**(4), 1–12 (2016). https://doi.org/10.1145/2897824.2925906

24. Kwiatkowski, A., Alvarado, E., Kalogeiton, V., Liu, C.K., Pettré, J., van de Panne, M., Cani, M.P.: A survey on reinforcement learning methods in character animation. Comput. Graph. Forum **41**(2), 613–639 (2022). https://doi.org/10.1111/cgf.14504

25. Kwon, T., Lee, Y., Van De Panne, M.: Fast and flexible multilegged locomotion using learned centroidal dynamics. ACM Trans. Graph. **39**(4) (2020). https://doi.org/10.1145/3386569.3392432

26. Lee, J., Shin, S.Y.: A hierarchical approach to interactive motion editing for human-like figures. In: Proceedings of the 26th Annual Conference on Computer Graphics and Interactive Techniques, SIGGRAPH'99, pp. 39–48. ACM Press/Addison-Wesley Publishing Co., USA (1999). https://doi.org/10.1145/311535.311539

27. Lentine, M., Gretarsson, J.T., Schroeder, C., Robinson-Mosher, A., Fedkiw, R.: Creature control in a fluid environment. IEEE Trans. Vis. Comput. Graph. **17**(5), 682–693 (2011). https://doi.org/10.1109/TVCG.2010.108

28. Loper, M., Mahmood, N., Romero, J., Pons-Moll, G., Black, M.J.: SMPL: A skinned multi-person linear model. ACM Trans. Graphics (Proc. SIGGRAPH Asia) **34**(6), 248:1–248:16 (2015)

29. Marion, J.L., Wimpey, J.: Assessing the influence of sustainable trail design and maintenance on soil loss. J. Environ. Manag. **189**, 46–57 (2017). https://doi.org/10.1016/j.jenvman.2016.11.074

30. Mourot, L., Hoyet, L., Le Clerc, F., Schnitzler, F., Hellier, P.: A survey on deep learning for skeleton-based human animation. Comput. Graph. Forum **41**(1), 122–157 (2022). https://doi.org/10.1111/cgf.14426

31. Müller, M., Heidelberger, B., Hennix, M., Ratcliff, J.: Position based dynamics. J. Vis. Commun. Image Represent. **18**(2), 109–118 (2007). https://doi.org/10.1016/j.jvcir.2007.01.005

32. Paliard, C., Alvarado, E., Rohmer, D., Cani, M.P.: soft walks: real-time, two-ways interaction between a character and loose grounds. In: Theisel, H., Wimmer, M. (eds.) Eurographics 2021—Short Papers. The Eurographics Association, Vienna, Austria (2021). https://doi.org/10.2312/egs.20211019

33. Paris, A., Peytavie, A., Guérin, E., Argudo, O., Galin, E.: Desertscape simulation. Comput. Graph. Forum **38**(7), 47–55 (2019). https://doi.org/10.1111/cgf.13815

34. Rahgoshay, C., Rabbani, A., Singh, K., Kry, P.G.: Inverse kinodynamics: editing and constraining kinematic approximations of dynamic motion. In: Proceedings of Graphics Interface 2012, GI'12, pp. 185–192. Canadian Information Processing Society, CAN (2012)

35. Raibert, M.H., Hodgins, J.K.: Animation of dynamic legged locomotion. SIGGRAPH Comput. Graph. **25**(4), 349–358 (1991). https://doi.org/10.1145/127719.122755

36. Shahbapoor, E., Pavic, A.: Measurement of walking ground reactions in real-life environments: a systematic review of techniques and technologies. Sensors (Switzerland) **17** (2017)

37. Wannop, J.W., Worobets, J.T., Ruiz, R., Stefanyshyn, D.J.: Footwear traction and three-dimensional kinematics of level, downhill, uphill and cross-slope walking. Gait & Posture **40**(1), 118–122 (2014). https://doi.org/10.1016/j.gaitpost.2014.03.004

38. Witkin, A., Kass, M.: Spacetime constraints. SIGGRAPH Comput. Graph. **22**(4), 159–168 (1988). https://doi.org/10.1145/378456.378507

Eduardo Alvarado is a postdoctoral researcher at Max Planck Institute for Informatics (Visual Computing and Artificial Intelligence). He completed his PhD in Character Animation and Computer Graphics at École Polytechnique, in the Visual Worlds: Temporal Analysis, Animation and Authoring (VISTA) group under the supervision of Prof. Damien Rohmer and Prof. Marie-Paule Cani, while being part of the Marie Skłodowska-Curie Innovative Training Network CLIPE, funded by the European Union Horizon 2020 framework. Prior to his PhD, he got his M.Sc. in Embedded Systems and AI at Albert-Ludwigs-Universität Freiburg and his B.Sc. in Electronics and Automation Engineering at Universidad Carlos III de Madrid. His research is centered on plausible, interactive, and multi-scale 3D animation (physically-based, kinematic) of virtual characters in dynamic and deformable environments, with focus on authoring tools for the entertainment industry (games, VR).

Oscar Argudo is Assistant Professor at the Computer Science department of Universitat Politècnica de Catalunya, working with the ViRVIG research group. He obtained his PhD in Computing from UPC in 2018, under the supervision of Carlos Andújar and Antonio Chica. His thesis focused on the creation of realistic natural scenarios, leveraging machine learning techniques and real data to improve procedural and example-based modeling algorithms. After that, he was hired as a postdoctoral researcher by the CNRS in the LIRIS laboratory in Lyon, working on procedural modeling of mountainous landscapes and the simulation of natural phenomena such as dunes, glaciers, and ecosystems. His current research project deals with the generation of hiking paths networks and the modeling of degradation effects caused by outdoor activities. He has published in journals such as ACM Transactions on Graphics and Computer Graphics Forum and presented in top conferences like SIGGRAPH Asia and Eurographics.

Damien Rohmer is Professor of Computer Science at Ecole Polytechnique, part of Institut Polytechnique de Paris. His research lies in the Computer Graphics field, and revolves primarily around 3D Modeling, Deformation, and Animation of virtual content, with a keen interest in Real-Time Efficiency, Interactivity and User Control. His previous research contributed to the Modeling and Animation of Virtual Character, Developable Surface, 3D Garment models, and to the Simulation of Natural Phenomena. His methodology typically couples procedural approaches and lightweight physics, with the use of appropriate geometrical representation featuring for instance hierarchical level of details and field-based representations. His work principally finds applications for entertainment production requiring efficiency and interactivity such as Animation Cinema, VFX, and Games, with publications in Graphics journals and venues including SIGGRAPH, Eurographics, SCA and MIG. He additionally enjoys collaboration with other disciplines such as Medical Sciences, Math, or Design.

Marie-Paule Cani is Professor of Computer Science at Ecole Polytechnique. Her research interests cover both Shape Modelling and Computer Animation. She contributed over the years to several high-level models for shapes and motion such as implicit surfaces, multi-resolution physically-based animation methods and hybrid representations for real-time natural scenes. Following a long-lasting interest in virtual sculpture, she has been recently searching for more expressive ways to create 3D content such as combining sketch-based interfaces with procedural models based on a priori knowledge or learning. She received the Eurographics outstanding technical contributions award in 2011, a Silver medal from CNRS in 2012, and was elected at the Academia Europaea in 2013. She was awarded the ERC advanced grant EXPRESSIVE (2012-2017) and joined the ACM SIGGRAPH Academy in 2019. She was elected at the French Academy of Sciences in 2020.

Nuria Pelechano is Associate Professor (Professor Agregat) at the HYPERLINK "http://www.upc.edu/" Universitat Politecnica de Catalunya (UPC) in Barcelona, and member of the research group HYPERLINK "http://www.virvig.eu/" ViRVIG. She is coordinator of the HYPERLINK "https://www.fib.upc.edu/en/studies/masters/master-innovation-and-research-informatics/curriculum/specializations/computer-graphics-and-virtual-reality" Computer Graphics and Virtual Reality specialty of the HYPERLINK "https://www.fib.upc.edu/en/studies/masters/master-innovation-and-research-informatics" MIRI master degree at the Facultat de Informàtica (UPC). She received her PhD in 2006 (as a Fulbright scholar) at the University of Pennsylvania (UPenn) under the supervision of Dr. Norman I. Badler. Afterwards she was a postdoctorate researcher at the TC Chan Center for Building Simulation and Energy Studies with Dr. Ali Malkawi and the Center for Human Modeling and Simulation with Dr. Norman I. Badler.